Available online at www.sciencedirect.com

SciVerse ScienceDirect

journal homepage: www.elsevier.com/locate/jmbbm

Research paper

Mechanical properties, electrochemical corrosion and *in-vitro* bioactivity of yttria stabilized zirconia reinforced hydroxyapatite coatings prepared by gas tunnel type plasma spraying

S. Yugeswaran[a], *C.P. Yoganand*[b], *A. Kobayashi*[a,*], *K.M. Paraskevopoulos*[c], *B. Subramanian*[a,d]

[a] *Joining & Welding Research Institute, Osaka University, Osaka 567-0047, Japan*
[b] *Department of Physics, Bharathiar University, Coimbatore-641046, India*
[c] *Department of Physics, Aristotle University of Thessaloniki, 54124 Thessaloniki, Greece*
[d] *CSIR-Central Electrochemical Research Institute, Karaikudi-630 006, India*

ARTICLE INFO

Article history:
Received 19 August 2011
Received in revised form
8 November 2011
Accepted 9 November 2011
Published online 26 November 2011

Keywords:
Hydroxyapatite
YSZ
Reinforcement
Plasma spray
Mechanical properties
Bioactivity

ABSTRACT

Yttria stabilized zirconia reinforced hydroxyapatite coatings were deposited by a gas tunnel type plasma spray torch under optimum spraying conditions. For this purpose, 10, 20 and 30 wt% of yttria stabilized zirconia (YSZ) powders were premixed individually with hydroxyapatite (HA) powder and were used as the feedstocks for the coatings. The effect of YSZ reinforcement on the phase formation and mechanical properties of the coatings such as hardness, adhesive strength and sliding wear rates was examined. The results showed that the reinforcement of YSZ in HA could significantly enhance the hardness and adhesive strength of the coatings. The potentiodynamic polarization and impedance measurements showed that the reinforced coatings exhibited superior corrosion resistance compared to the HA coating in SBF solution. Further the results of the bioactivity test conducted by immersion of coatings in SBF showed that after 10 days of immersion of the obtained coatings with all the above compositions commonly exhibited the onset of bioactive apatite formation except for HA+10%YSZ coating. The cytocompatibility was investigated by culturing the green fluorescent protein (GFP)-labeled marrow stromal cells (MSCs) on the coating surface. The cell culture results revealed that the reinforced coatings have superior cell growth than the pure HA coatings.

* *Correspondence to:* Joining and Welding Research Institute, Osaka University, 11-1 Mihogaoka, Ibaraki, Osaka 567-0047, Japan. Tel.: +81 6 6879 8694; fax: +81 6 6879 8694.
E-mail address: kobayasi@jwri.osaka-u.ac.jp (A. Kobayashi).

1751-6161/$ - see front matter © 2012 Published by Elsevier Ltd
doi:10.1016/j.jmbbm.2011.11.002

1. Introduction

Chemical structure of hydroxyapatite (HA) is very close to human bone which makes it compatible with the tissue of the human body. Its good biocompatibility causes it to be extensively used in many prosthetic applications, especially as a porous material for optimal bone in growth (Geesink et al., 1987). Currently, this material is being deposited on bio-inert metallic implants and used as recovery parts in human body. Many methods are used to deposit the HA coatings on the surface of metallic implants such as conventional press-and-sinter method, ion beam sputtering, electrophoretic deposition, RF-magnetron sputtering, pulse laser melting, physical vapor deposition and electrochemical deposition (Ding et al., 2000). However plasma spraying is the most widely used technique due to its process feasibility such as easy operation and bulk production. Plasma sprayed hydroxyapatite with metallic alloy, exhibits both biocompatibility and good mechanical properties thereby making it more suitable for surgical implants (Nie et al., 2000; Chon and Chang, 2002). However, this technique has severe limitations because the high temperature and rapid cooling associated with this process yields a variety of phases and lower crystallinity of HA (Sun et al., 2001). With decreasing crystallinity, the dissolution rate of the phosphorus compounds such as β-tricalcium phosphate (β-TCP) and tetra calcium phosphate (TTCP) is much faster than single phase HA thereby leading to implant instability (Sergo et al., 1997). Hence, plasma sprayed HA coated implants essentially consist of a mixture of crystalline, amorphous, and non-apatite phases such as $Ca_3(PO_4)_2$ (TCP), $Ca_4(PO_4)_2O$ (TTCP) or even CaO. Also, thicker coatings produced by plasma spray often exhibited porosity that weakened the interfacial strength and provided an easy fracture path for adhesion failure and reduced the corrosion resistance (Ahn et al., 2002).

It has been well documented that plasma sprayed coatings suffer from low adhesion between coating and the substrate, as well as low cohesion within the coating microstructure (Nal and Sordelet, 2000). Previously many researchers suggested that the weak lamellar splat layer of the HA coating microstructure could be improved through plasma spray processing by means of reinforcing second phase such as ceramics, metals, alloys and or composite along with HA (Weng et al., 1994; Morks, 2008; Gurbhinder et al., 2011; Xuebin et al., 2000). Among these second phases, reinforcing of Yttria stabilized zirconia (YSZ) can significantly enhance the mechanical properties of HA coatings due to its high strength and stress-induced phase transformation toughening nature (Witek and Buttler, 1985; Lee et al., 2004). Also, the bioactivity of HA coating improved considerably while using YSZ as the second phase because of its biocompatibility merit (Gu et al., 2004). Reports on plasma sprayed YSZ reinforced HA coatings revealed that the addition of YSZ to HA produced better mechanical properties than those of bulk HA alone (Chou et al., 2002; Fu et al., 2002).

Meanwhile, fundamental understanding of the relationship between the plasma spray processing and coating characteristics is a key factor for obtaining HA and or HA reinforced coatings with predictable properties and performance for implant applications. Variations in the deposition parameters can lead to different phase compositions, crystal structure and microstructures, which results in alteration of major coating properties. The heterogeneity of the plasma jet affects the quantity of air entrainment and heat transfer rates to particles while in-flight through the plasma zone. Thus, it is difficult to produce a coating with the desired coating characteristic by using conventional plasma spraying method. Furthermore, there is generally a concern over the consistency and reliability of the coating quality.

Therefore, in this present study a high-power plasma jet known as gas tunnel type plasma torch (GTTP), developed in Osaka University, was used to produce HA and YSZ reinforced HA coatings on stainless steel substrate. This unique technique was previously used to deposit high quality ceramic coatings due to its high power and high spraying efficiency (Arata and Kobayashi, 1986). The advantages, unique features and as well as the influences of the processing parameters on the coating properties are well documented in the previous publications (Morks and Kobayashi, 2008, 2007). In the present study, phase and microstructure formation of the GTTP sprayed HA and YSZ reinforced HA coatings was investigated. The effect of YSZ reinforcement on the coating's mechanical properties such as adhesive strength, hardness and sliding wear rate was examined. Furthermore, electrochemical corrosion behavior and in-vitro bioactivity of the coatings in conventional simulated body fluid (c-SBF) solution was tested. The cytocompatibility of the coatings was also investigated by culturing green fluorescent protein (GFP)-labeled marrow stromal cells (MSCs) on its surface.

2. Experimental procedure

2.1. *Plasma spraying*

Specially designed gas tunnel type plasma spray torch was employed to form coatings with controlled microstructure under optimized operating conditions. The typical torch operating parameters are listed in Table 1. Schematic of the gas tunnel type plasma jet and splats formation during spraying is shown in Fig. 1. Commercially available hydroxyapatite (HA) and 8 wt% yttria stabilized zirconia (YSZ) powders from Pawlex Ltd. Tokyo, Japan with an average particle size of 10–45 μm and 10–30 μm respectively were used for preparing the coatings. The microstructure of the HA particles was spherical in shape whilst the YSZ particles was angular and both the powders had relatively high purity and were well crystallized. The HA powder was mechanically milled individually with three different weight proportions of YSZ (10, 20 and 30 wt%) and the mixtures were used as the powder precursor for spraying. Herein, the powder precursor was fed externally at the exit of the nozzle in order to avoid decomposition process due to melting in high temperature plasma jet. The coating was formed on the surface of a 316 L stainless steel substrate whose dimensions were 50 × 50 × 2.5 mm. Prior to spraying, the substrate surface was grit blasted with alumina for surface roughening and it was followed by cleaning using acetone. Furthermore, the operating parameters used in the present coating were selected in order to get coating with thickness of around 300–400 μm with significant porosity and also taking caution that there is minimal deviation from the initial stoichiometric ratio.

Table 1 – Plasma spraying conditions and sample code.

Powder ratio (wt%)		Nomenclature of coatings	Operating parameters	
HA	8YSZ			
100	0	HA	Arc power:	15 kW
			Spraying distance:	60 mm
90	10	HZ10	Working gas flow rate (Ar):	180 l/min
80	20	HZ20	Carrier gas flow rate (Ar):	10 l/min
			Powder feed rate:	15 g/min
70	30	HZ30	Traverse number:	16 times

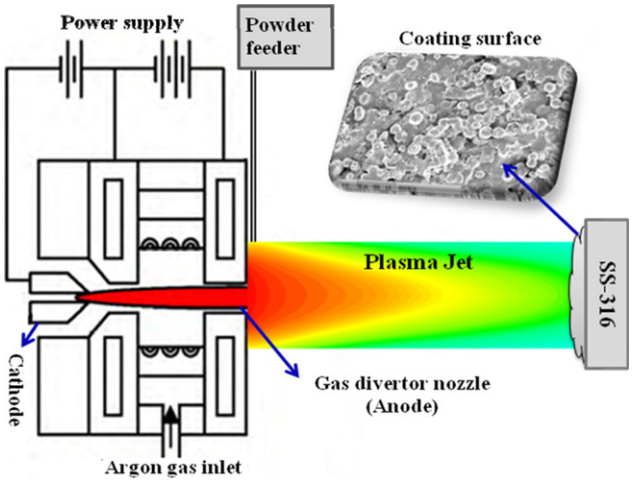

Fig. 1 – Schematic of gas tunnel type plasma spray torch and coating formation.

2.2. *Phase, microstructure and mechanical characterization*

Phase constituents of the coatings were identified using JEOL JDX-3530M X-ray diffractometer with Cu-Kα radiation source at a voltage of 40 kV and a current of 40 mA. The microstructures of the coatings were examined by ERA8800FE scanning electron microscope equipped with energy dispersive X-ray spectroscopy. Porosity of the coatings was evaluated by image analyzing method using computerized optical microscope. Peel off test method was used to determine the adhesive strength of the coatings. The standard specimens with dimensions of 1 × 1 cm were used for the study. Hardness tests were performed on polished cross-sections of the coatings by using Akashi AAV-500 series hardness tester. The load used was 490.3 mN and the load time was 20 s. Each hardness value is the average of 5 readings. For the evaluation of the friction and wear resistance of the different coating specimens, a ball-on-disk tribometer was used. The measurements were carried out at room temperature in laboratory air with a relative humidity of about 60%. Alumina balls, 5 mm in diameter, were used as the counterbody. Prior to each test the samples and the balls were cleaned with ethanol. The tests were performed using three different normal loads such as 10, 20 and 30 N, corresponding to Hertzian stresses within 0.68–1.05 GPa. In all the tests, the sliding speed was maintained at a constant value of 0.2 ms^{-1} by adjusting the rotation speed of the disk and the diameter of the wear track. The duration of sliding was 10,000 rotation cycles. Wear volumes of the coating specimens were measured accurately using a three-axis profilometer (Taylor Hobson) equipped with a PC. Wear tracks were mapped and the wear volume was calculated accordingly. The results reported in this paper are in the form of Archard's specific wear rate (mm^3/N m), calculated by the following formula:

$$\text{Specific wear rate} = \frac{V}{F \times S} \quad (1)$$

where V is the volume worn away in mm^3, F is the normal load in N, and S is the sliding distance in meter. Each specified test was conducted in three different areas of the coating surface in order to obtain statistical working results.

2.3. *Electrochemical corrosion analysis*

A potentiostat (Autolab PGSTAT galvanostat/potentiostat) was employed to realize the electrochemical corrosion behavior of the coatings in conventional simulated body fluid (SBF) electrolyte (Huang et al., 2005). For this purpose, conventional three-electrode cell was used with the counter electrode made of a platinum rod and a saturated calomel electrode (SCE) as the reference electrode and the sample as the working electrode. The test electrolytes, SBF solutions were prepared at pH value of 7.4 and the test specimens were masked with 3 M scotch to expose a constant surface area of 1 cm^2. In order to establish the open circuit potential (OCP), prior to the polarization measurements, the samples were immersed in the solution for about 60 min. The applied alternating potential had root mean square amplitude of 10 mV on the OCP. After getting the stable OCP, the upper and lower potential limits of linear sweep voltammetry were set at +200 and −200 mV respectively with reference to OCP. The sweep rate was 1 mV s^{-1}. The corrosion potential E_{corr}, corrosion current I_{corr} and corrosion rate were determined by the Tafel extrapolation method. Impedance measurements were conducted using a frequency response analyzer and the spectrum was recorded in the frequency range of 10 mHz–100 kHz.

2.4. *In-vitro bioactivity analysis*

All samples were smoothed by using mechanical polishing machine with alumina sheet before immersion in the solution and the in-vitro bioactivity of all the coated samples was tested for 5, 10 and 15 days in SBF solution prepared as described in literature (Kokubo et al., 1990). Fourier Transform Infrared Spectroscopy (FTIR) was used to characterize the surface of the coatings after immersion in the SBF solution for different periods along with XRD. Here, FTIR transmittance spectra were obtained using IFS 113 V, Bruker spectrometer in NIR region with a resolution of 2 cm^{-1}. The topographical evaluation and elemental analysis of the samples before and after immersion in SBF were performed by a Philips XL40 scanning electron microscope with associated energy dispersive X-ray spectrometer (SEM/EDS).

Further to investigate the cytocompatibility of the coated samples, green fluorescent protein (GFP)-labeled marrow

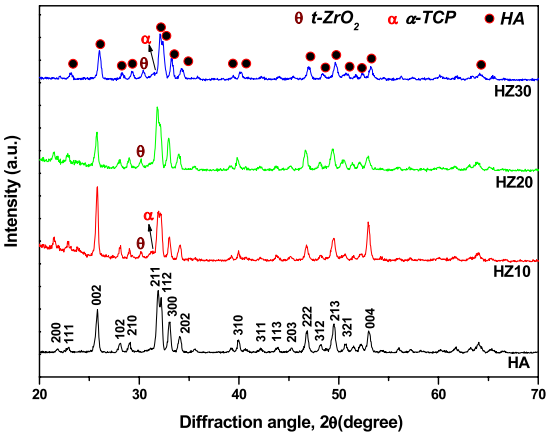

Fig. 2 – X-ray diffraction pattern of gas tunnel type plasma sprayed HA and YSZ reinforced HA coatings.

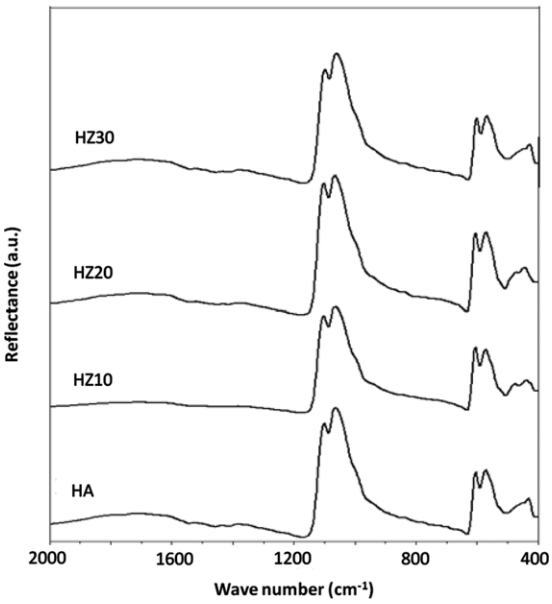

Fig. 3 – Fourier transform infrared spectra of gas tunnel type plasma sprayed HA and YSZ reinforced HA coatings.

stromal cells (MSCs) (the GFP transgenic SD rats were provided by Dr. X. Huang, Department of orthopedics, Xijing Hospital) of male SD rats were cultured on the coating surfaces. 5×10^4 cells were added to each well of a 24-well plate. Each well contained a specimen from different groups. After being cultured for 24 and 48 h, the specimens were removed from the plates and observed under fluorescence microscopy (TE2000, Nikon, Japan) and scanning electron microscopy (S-3000 N, Hitachi Japan).

3. Results and discussion

3.1. *Structural and mechanical characterization*

The XRD patterns of the as-sprayed coatings are shown in Fig. 2. The XRD spectra showed that the as-sprayed pure HA coating retained its crystalline HA phase similar to the initial feed stock HA powder, even though there existed a possibility for occurrence of decomposition during its in-flight in high temperature plasma zone by the following reaction mechanism (Lorcardi et al., 1993):

$$Ca_{10}(OH)_2(PO_4)_6\{HA\} \rightarrow 2Ca_3(PO_4)_2\{TCP\} + Ca_4P_2O_9\{TTCP\} + H_2O. \quad (2)$$

Conventional plasma sprayed HA coatings generally contain secondary phases such as α-TCP, β-TCP, TTCP, amorphous calcium phosphate (ACP) and CaO because of the severe decomposition of the in-flight apatite induced by the high temperature plasma jets. On the contrary, in the present case the decomposition processes of in-flight HA could be well controlled by means of selective operating parameters and unique nature of GTTP jet. However, the addition of ZrO_2 with HA slightly affected the crystallinity of HA and produced α-TCP as an additional phase along with tetragonal phase ZrO_2, which is shown in the XRD pattern of HA–ZrO_2 composite coatings.

Generally the decomposition of HA produces α-TCP but it is an unstable phase at room temperature and hence obviously gets transformed to β-TCP, which is a stable phase at room temperature. However the phase analysis of the HA–ZrO_2 composite coating obtained in this study exhibited α-TCP phase instead of β-TCP, which was due to the rapid solidification behavior of the gas tunnel type plasma jet that permitted the formation of a stable α-TCP. Similar kind of result was previously reported during the formation of conventional plasma sprayed HA and its composite coatings (Morks and Kobayashi, 2007; Chang et al., 1997). Moreover, in this study the other decomposition phases such as TTCP and CaO phases were not found.

The GTTP sprayed HA–ZrO_2 composite coatings exhibited the presence of characteristic FTIR peaks like that of synthetic hydroxyapatite (HA) as reported in literature (Muller et al., 2007) and as shown in Fig. 3. From the spectra, it is found that all these coatings showed a wide peak at 1050–1100 cm^{-1} which is attributed to the stretching vibrational mode of P–O of PO_4 group. In addition, the double peaks at 570 cm^{-1} and 601 cm^{-1} attributed to the bending vibrational mode of P–O bond were observed. In the case of ZrO_2 content, FTIR spectra are known to be present, as most oxides, a broad peak under 700 cm^{-1} or multiple smaller ones in the same spectral area depending on the crystal growth of zirconia (Damyanova et al., 2008). Considerably, the small amount of ZrO_2 used in these composites, made it difficult to distinguish between the peaks attributed to HA and ZrO_2 as observed from FTIR spectra.

Scanning electron micrographs of top surfaces of as-sprayed HA and YSZ reinforced HA coatings are shown in Fig. 4. It is observed from the micrographs that both the kinds of coating surfaces have some partially melted and few unmelted particles and there are only few micro cracks, which is inherent to the plasma spray deposition mechanism. Plasma sprayed ceramic coatings are generally porous and this characteristic is beneficial to the biomedical application involving the mechanical fixation through bone in growth (Chou and Chang, 2002; Fu et al., 2002). Meanwhile, the formation of such pores severely affects the mechanical properties of the coating and as well instigates swift failure. Herein the investigation results shown in Fig. 5 reveal that the porosity of HA coating is higher and with the addition

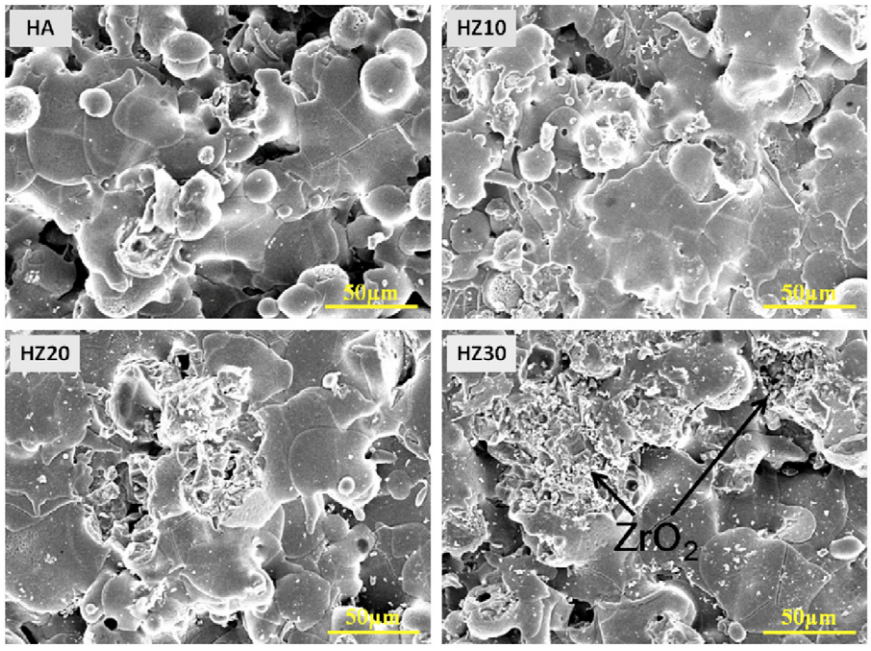

Fig. 4 – Surface morphology of gas tunnel type plasma sprayed HA and YSZ reinforced HA coatings.

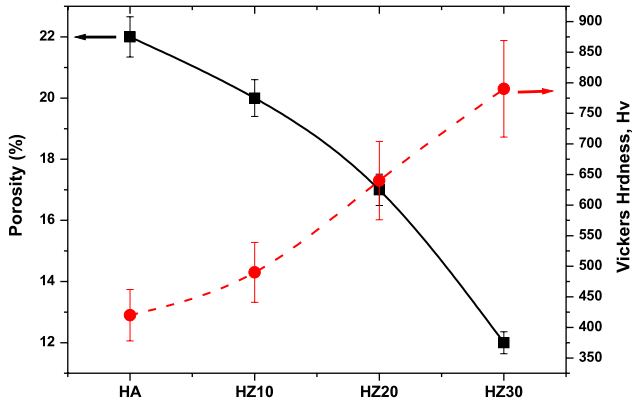

Fig. 5 – Porosity and microhardness of gas tunnel type plasma sprayed coating.

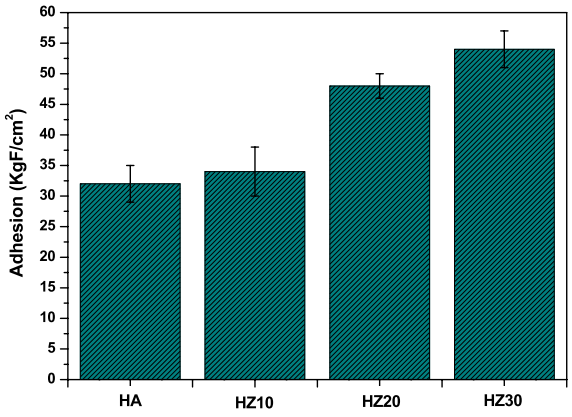

Fig. 6 – Adhesive strength of gas tunnel type plasma sprayed HA and YSZ reinforced HA coating.

of YSZ it gets reduced compared to pure HA coating. This may be attributed to the small size of the reinforcing material which fills the pores in the coating microstructure. Similar effect of reinforcement in the form of decreased porosity was observed by Morks and Kobayashi (2007) and Gurbhinder et al. (2011) while reinforcing ceramic in pure HA coatings. The HA coatings with and without YSZ have nearly the same thickness of around 300–400 μm.

Existence of direct relationship between the hardness and the porosity of the plasma sprayed coatings, i.e. the lower the porosity higher the coating hardness, was impeccably reflected in the present coating results as well. The results from Fig. 5 shows that the hardness of the coatings increase while increasing the content of reinforced YSZ in HA which is mainly due to the formation of dense coatings with low porosity. The presence of unmelted particles and pores inside the coating microstructure play a vital role in the bonding strength of the coating. Fig. 6 shows the adhesive strength of the HA coatings as a function of reinforced YSZ content and the results indicate that the adhesive strength of the HA coatings significantly improved with the addition of YSZ to HA. Astonishingly, 30% YSZ in HA doubled the adhesive strength of the coating compared with that of the pure HA coatings. Consistent formation of micro-cracks inside the coating layer due to the thermal stress and residual coating stresses arising due to the high solidification rate; also the formation of amorphous layer over the surface of the splats and interface during the impinging of in-flight droplets to the substrate can reduce the adhesive strength because of the brittle nature. The reinforcement of YSZ decreases the solidification rate of the in-flight HA particles and prevents the formation of amorphous interface layer thereby causing enhancement of the adhesive strength in HA–YSZ composite coatings. Earlier report from Chou and Chang proves 2002 that

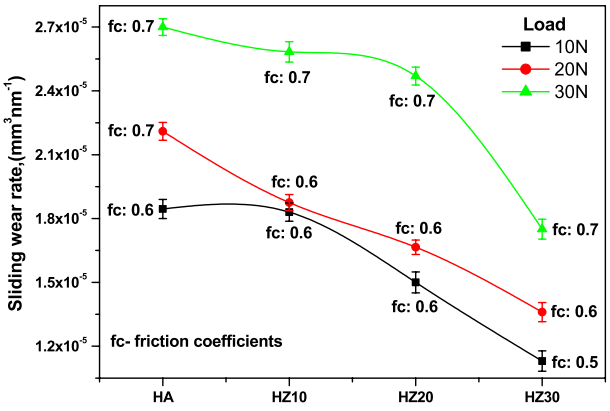

Fig. 7a – Sliding wear rate and friction coefficient of gas tunnel type plasma sprayed HA and YSZ reinforced HA coatings at three different loads (10, 20, 30 N).

reinforcement of ZrO_2 particles in HA coatings considerably enhanced the bond strength and cohesive strength on Ti alloy substrates.

The effect of YSZ reinforcement on the sliding wear rate and the friction coefficient of the HA coatings at three different loads such as 10, 20 and 30 N is shown in Fig. 7a. It was found that the sliding wear rate got considerably decreased with respect to YSZ reinforcement. In case of HZ30 coating, the result revealed minimum wear rate at all the load conditions. This decreasing trend was mainly caused by the decreased porosity and enhancement of the coating hardness with respect to YSZ reinforcement. The summary of the previous research reports correlate the wear volume loss and hardness of the materials, which are inversely proportional to each other (Rabinowicz, 1965). The results obtained in this study are in well agreement with this relationship and exhibit that the wear rate got drastically reduced on increasing the reinforcement material (Younesi et al., 2010; Mazzocchi et al., 2008).

The 3-dimensional wear track images of the HA and HZ30 coatings tested at 10 and 30 N are shown in Fig. 7b. It showed that the depth of the wear grooves on HZ30 coating surface was least and there was well controlled structure rather than pure HA coating surface at 10 N load and also similar structure was retained in 20 N load. Hence the observation from the wear track confirmed the abrasive wear mechanism on the surfaces of HA and YSZ reinforced HA coatings at low wear load conditions and as well as demonstrated that the reinforced materials sustain the low wear loads thus resulting in minimal wear rates (Zhang and Alpas, 1993).

Meanwhile, it was found that the sliding wear rate of all the coatings significantly increased by increasing the wear load, which can be related to the changes in wear mechanism on the coating surfaces. The order of increasing wear rate is relatively higher in pure HA coating rather than HZ30 coating at high load applied. Herein, instead of abrasive wear mechanism, adhesive and or third body wear mechanism can also occur on all the coating surfaces. At high wear load, partially or un-melted HA particles are easily disconnected from its lamella microstructure due to its feeble bonding strength. Also continuous motion of the surfaces causes breaking of the bond junctions and creates wear of particles from the weaker materials; this is the stand point of adhesive wear mechanism during sliding at high load conditions. Also, occasionally the resulting adhesive wear particles can induce the third body wear mechanism. The reinforced YSZ considerably enhances the cohesive strength of the splat in lamella microstructure and thus prevents the removal of HA from the coating microstructure. Furthermore, the reinforcement can considerably reduce the porosity in the coating microstructure; this has been clearly illustrated in Fig. 5. Generally, the volume fraction of porosity and the pore size distribution have considerable effect on the sliding wear behavior of plasma sprayed coatings. However, the constructive and unfavorable role of porosity in wear resistance strongly depends on the wear conditions. For example, presence of porosity in the coating microstructure provides a considerable

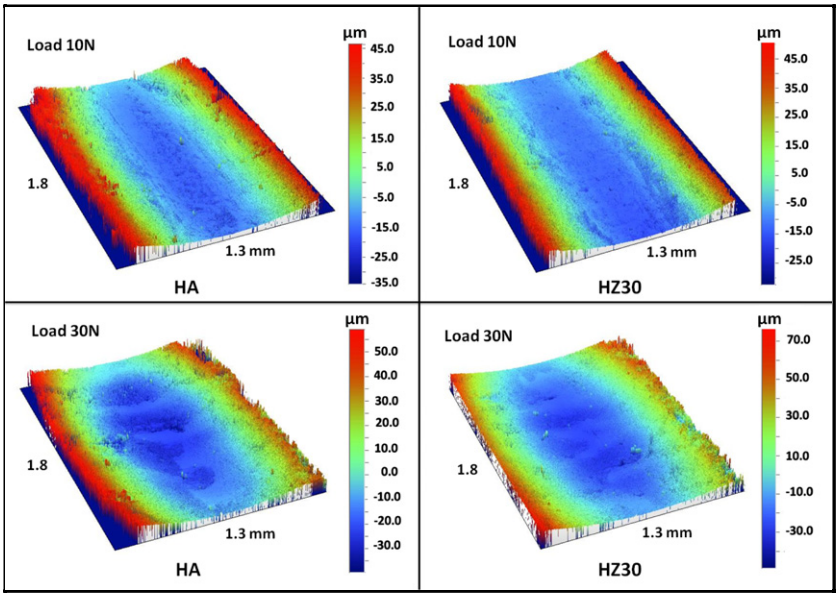

Fig. 7b – 3-dimensional image of wear track surface of HA and HZ30 coatings at 10 and 30 N wear load.

advantage in lubricated wear conditions because it acts as lubricant reservoirs or lubricating channels. In contrast, while in dry sliding wear conditions, the porosity can promote surface and subsurface cracking and also favor the occurrence of granular wear particles in the contact area (Lim and Brunton, 1986). Hence due to these reasons, YSZ reinforced HA coatings exhibit superior wear resistance than HA coatings in all the load conditions. However, the resulting subsurface deformation on all the coatings during wear at 30 N wear load was inevitable, but it could be well controlled in 30% YSZ reinforced HA coating.

Fig. 7b shows the 3-dimensional image of wear track surface of HA and HZ30 coatings at 30 N wear load condition as fact of surface deformation due to the combined wear mechanism. At low wear load, the subsurface deformation is negligible due to the type of wear mechanism and grooves formation, but at high wear load, the depth of the grooves formed from abrasive particles of the coating surface is high and thus encourages the deformation over the surface. Moreover, the overall observation from the wear track surface of HA and HZ30 coatings at two different wear load conditions provides more authentication of the change in wear mechanism with respect to applied wear loads.

Fig. 7a presents the average friction coefficient of HA and YSZ reinforced HA coatings for different wear loads. Friction coefficient was observed to be hovering around 0.5–0.7. It was observed that with increase in normal load, friction coefficient decreases, i.e. direct proportionality exists between the applied normal load and the measured friction coefficient. This rise in the friction coefficient can be attributed to the changes in wear mechanism with respect to applied loads. It was also observed that the load effect on friction coefficient was less intense than that on the wear rate. Also the YSZ reinforcement cannot significantly influence the friction coefficient values of the coatings even though it plays a vital role in decreasing the wear rates. However, HZ30 coating has relatively low friction coefficient than pure HA coating at 10 and 20 N load conditions. This slight variation may occur mostly because of the low porosity of the reinforced coating. It was earlier mentioned that, removal of material by pull-out from near the pore or in micro cracking regions in splats leads to surface roughness. As a result, friction increases substantially, favoring the occurrence of wear particles in the contact area. In addition to this, the relatively smooth sliding surface obtained in the reinforced coating surface leads to an increase in the cohesive force between the two contact surfaces. The present investigation showed that YSZ reinforced HA coatings has high hardness and low porosity, which results in wear rate reduction. This implies that low porosity and high hardness are mainly responsible for the low wear rate in plasma sprayed coatings. This tribological property examination cannot perfectly simulate the movement in the real biological system. However, the sliding contact test allows forecasting the highest wear resistance and friction coefficient of HA coating with respect to YSZ reinforcement under static conditions.

3.2. *Electrochemical corrosion analysis*

The potentiodynamic polarization experiments provided an idea of the electrochemical activity of the coatings. The potentials were either anodic or cathodic with respect to the primary electrochemical process occurring on the surface as indicated by the polarization curves. The potentiodynamic polarization curves obtained for the HA, HZ10, HZ20 and HZ30 coatings in simulated body fluid (SBF) solution are shown in Fig. 8. In the plot of potential versus log *i*, extrapolation of linear line to corrosion potential gives a straight line and the slope gives both b_a and b_c and the intercept gives the corrosion current. The corrosion potential (E_{corr}) and the corrosion current density (I_{corr}) for these coatings were calculated from the polarization curves and are presented in Table 2. The corrosion potential of the HA coated steel is about −0.308 V. The HZ30 sample, when compared to HA coating, shows a shift towards the positive side to −0.245 V. It can be seen that the composite coatings improved the corrosion resistance of the specimens by decreasing the I_{corr}. For the HA coating, corrosion current density is about 3.236×10^{-7} A cm^{-2}, which decreases to 0.170×10^{-7} A cm^{-2} for HZ30 coating.

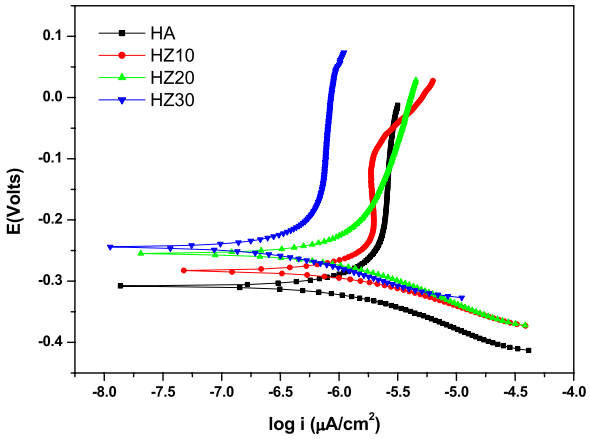

Fig. 8 – The potentiodynamic polarization curves of HA and YSZ reinforced HA coatings in simulated body fluid (SBF) solution.

The electrochemical impedance spectrum of the system was measured in the same three electrode assembly, as used for the potentiodynamic polarization experiments. Impedance measurements were made at open circuit potential (OCP) applying an AC signal of 10 mV in the frequency range of 10 mHz–100 kHz. The impedance results obtained from the Nyquist plots of the coating samples used for corrosion tests in SBF solution are shown in Table 2 and Fig. 9. The interpretation of AC impedance data using the Nyquist plot can become slightly complicated, particularly when small defects are present and short circuit the resistance of the coating, a situation which approximates to the equivalent circuit model shown in Fig. 9 (inside). When the sample is immersed in the electrolyte the defects such as micro cracks in the coating provide the direct diffusion path for the corrosive media. In this process the galvanic corrosion cells are formed and localized corrosion dominates the corrosion process. The electrochemical interface can be divided into two sub interfaces: electrolyte/coating and electrolyte/substrate. Theoretically the Nyquist plot for such a system should exhibit two responses, a high frequency response due to the parallel arrangement of coating capacitance (Cc), and pore resistance (Rpo), and a lower frequency response due to the corrosion

Table 2 – Corrosion results of HA and YSZ reinforced HA coatings in SBF solution.

Coatings	E_{corr} (V)	b_a (V dec^{-1})	b_c (V dec^{-1})	I_{corr} ($\times 10^{-7}$ A cm^{-2})	Corrosion rate (mpy $\times 10^{-3}$)	R_{ct} (Ω cm^2)	C_{dl} ($\times 10^{-10}$ F/cm^2)
HA	−0.308	0.025	0.047	3.236	3.691	12 602	5.6158
HZ10	−0.283	0.020	0.027	2.636	3.007	20 620	3.5101
HZ20	−0.255	0.015	0.011	0.886	1.011	28 121	2.3993
HZ30	−0.245	0.009	0.009	0.170	0.194	50 326	0.2212

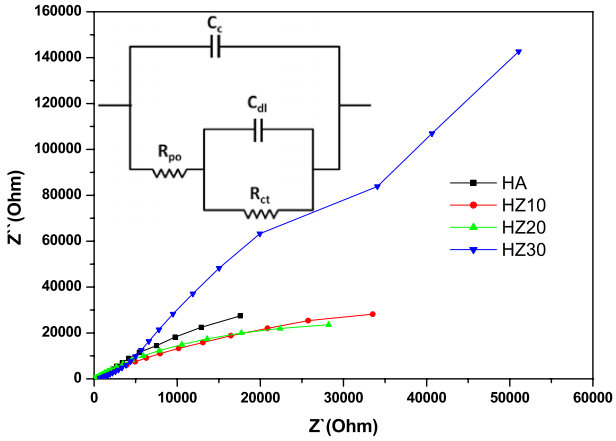

Fig. 9 – Nyquist plots and equivalent circuit of the HA and YSZ reinforced HA coatings.

cell formed at the base of the defect. The single semicircle behavior obtained for the samples is believed to be due to the short exposure time (60 min), which is not sufficient to reveal the degradation of the substrate (Liu et al., 2001).

The increase in R_{ct} values and decrease in C_{dl} values as shown in Table 2 for the HA with composite coatings system confirm their better corrosion resistance property compared to the HA coating. This suggests that significant improvement in corrosion resistance in human body environment can be achieved with the HA with YSZ. The defects such as porosity and voids formed during the deposition of the plasma sprayed coatings could weaken the material and provide easy fracture path for adhesion failure. In a composite coating, as the number of interfaces increase, more micro-pores are blocked which improves the corrosion resistance of the composite coatings.

From the polarization test results, the protective efficiency, P_i (%) of the films can be calculated by Eq. (1):

$$P_i(\%) = \left[1 - \left(\frac{i_{corr}}{i_{0\ corr}}\right)\right] \times 100 \quad (3)$$

where i_{corr} and $i_{0\ corr}$ indicate the corrosion current density of the film and substrate, respectively (Yoo et al., 2008). The protective ability of the coating increased with the incorporation of YSZ into the HA coatings. The HZ30 film showed the highest protective efficiency of 94.8% caused by the lowest corrosion current density of 0.17 $\times 10^{-7}$ A cm^{-2}.

3.3. *Formation of apatite layer after immersion in SBF*

In the case of HA coating, SEM microphotographs (Fig. 10(a)) could not reveal the formation of apatite on the surface of the samples after 5 days of immersion, but after 10 days of immersion in SBF, onset of apatite formation was found on the surface of the HA coatings which later intensified in the form of surface granules for 15 days of immersion. These results were confirmed by EDS analysis that showed a mean molar Ca/P ratio of about 1.78 for samples immersed in SBF for 10 and 15 days compared to the initial samples whose Ca/P ratio was at about 1.99. The SEM microphotographs (Fig. 10(b)) of HZ10 composite coatings did not quite clearly reveal the formation of apatite on the surface of the samples after 5 days of immersion. It was confirmed after 10 and 15 days that the apatite layer was formed on the coating surface. The EDS analysis revealed a mean molar Ca/P ratio of about 1.85 for samples immersed in SBF for 15 days compared to the samples immersed for 0,5 and 10 days whose mean molar Ca/P ratio was about 1.98, 2.1 and 1.95 respectively.

Apatite formation on the surface of the samples immersed in SBF for 5 days was not revealed by SEM microphotographs (Fig. 10(c)) of HZ20 samples. After 10 days of immersion, the onset of apatite formation on the surface of the coatings was revealed, while after 15 days an apatite layer was formed on the surface of the coatings. These findings were confirmed by EDS analysis which indicated that for samples immersed in SBF for 0 days the mean molar Ca/P ratio was about 2.0, after 5 days 1.99, after 10 days 1.83 and after 15 days 1.79. The SEM microphotographs of HZ30 did not indicate the onset of apatite formation on the surface of the samples earlier than 5 days of immersion, as shown in Fig. 10(d). Only after 10 days of immersion the onset of apatite formation was revealed on the surface of the coating and after 15 days of immersion the expansion in the formation of apatite on the surface of the coatings was found. In addition, EDS analysis presented a mean molar Ca/P ratio of approximately 2.1 for samples before immersion in SBF, 1.77 for the samples immersed for 10 days in SBF and 1.73 for those immersed for 15 days.

In the case of all the types of coating samples, the onset of biological apatite formation on their surface was detected after 10 days in SBF solution, while concerning HZ10 samples, there was no indication that an HCAp phase was crystallized on its surface even after 15 days. This could probably be attributed to the lack of homogeneity on the surface of HZ10 coatings, since the starting materials may behave differently during the deposition on the substrate by the plasma spray method (Blahoslav et al., 1999). The apatite formation spectra of the present plasma sprayed coatings are in good agreement with the standard biological apatite spectrum (Nancy et al., 1991; Dong and Yu, 2011).

It was observed from the FTIR spectra of HA coatings that after 5 days of immersion in SBF the onset of apatite formation did not occur since there was no significant alteration of the spectra, the FTIR spectra for 10days of immersion showed a slight variation in the double broad peak at 1050–1100 cm^{-1} indicating the preset of bioactivity

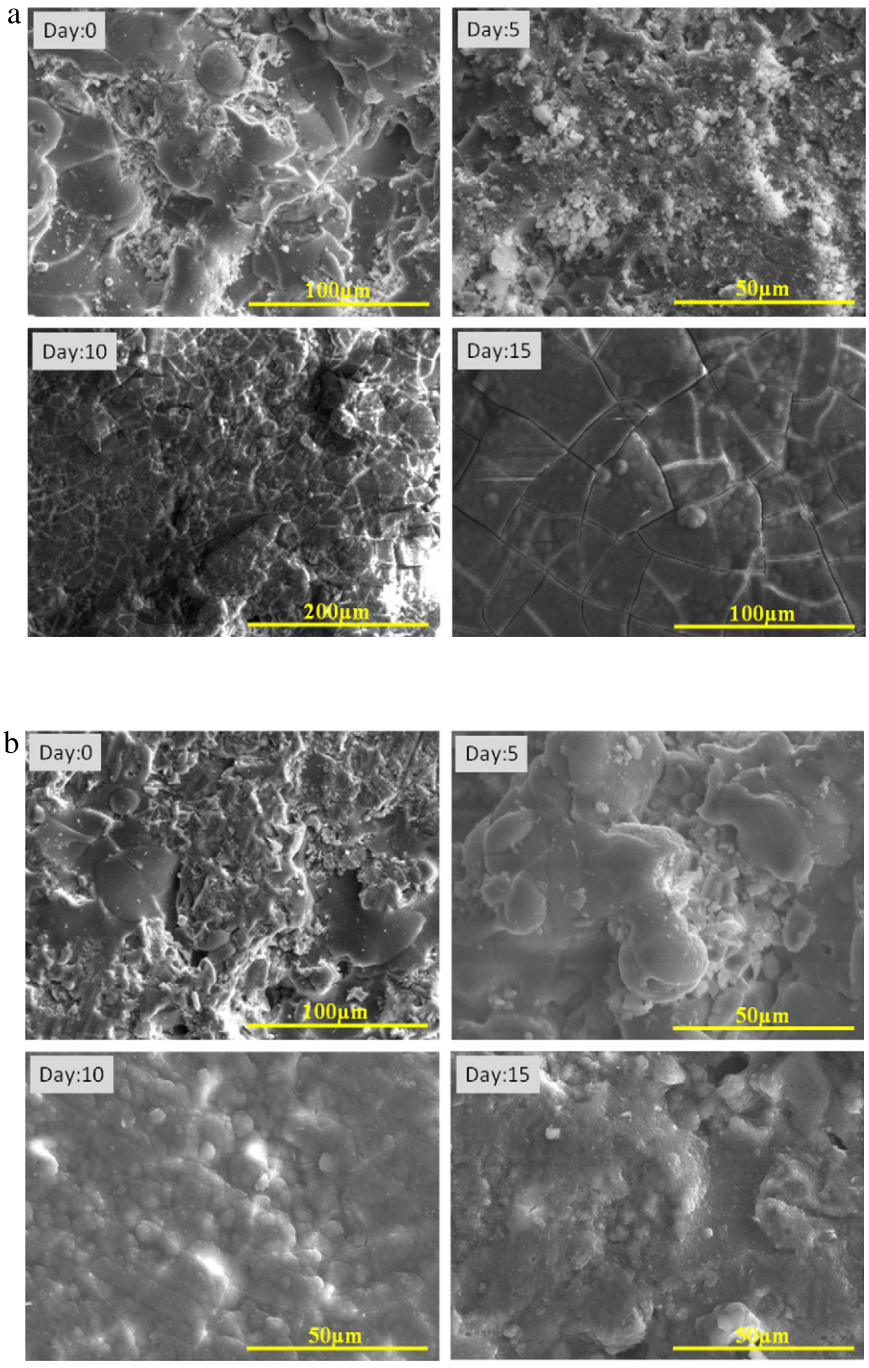

Fig. 10 – Scanning electron microscope images of coatings after immersion in SBF solution at 0, 5, 10 and 15 days of immersion: (a) HA; (b) HZ10; (c) HZ20; (d) HZ30.

but after 15 days of immersion in SBF solution, the shifting and the sharpening of the broad peak at 1050–1100 cm^{-1}, attributed to the stretching vibrational mode of P–O of PO_4 group; quite clearly indicated the formation of an amorphous Ca–P phase (Chatzistavrou et al., 2006). The FTIR spectra of HA, HZ10, HZ20, HZ30 coatings after 10 days of immersion in SBF are shown in Fig. 11. The FTIR spectra of HZ10 coatings did not indicate the onset of apatite formation on the surface of the sample even after 15 days of immersion. The FTIR spectra of HZ20 coatings for 5 days of immersion did not indicate the onset of apatite formation, but for the samples immersed for 10 days in SBF, the shifting and the sharpening of the broad peak at 1050 cm^{-1}, was revealed whereas the FTIR spectra of HZ30 coatings after 10 days of immersion in SBF solution, indicated the formation of an amorphous Ca–P phase as confirmed by SEM–EDS analysis.

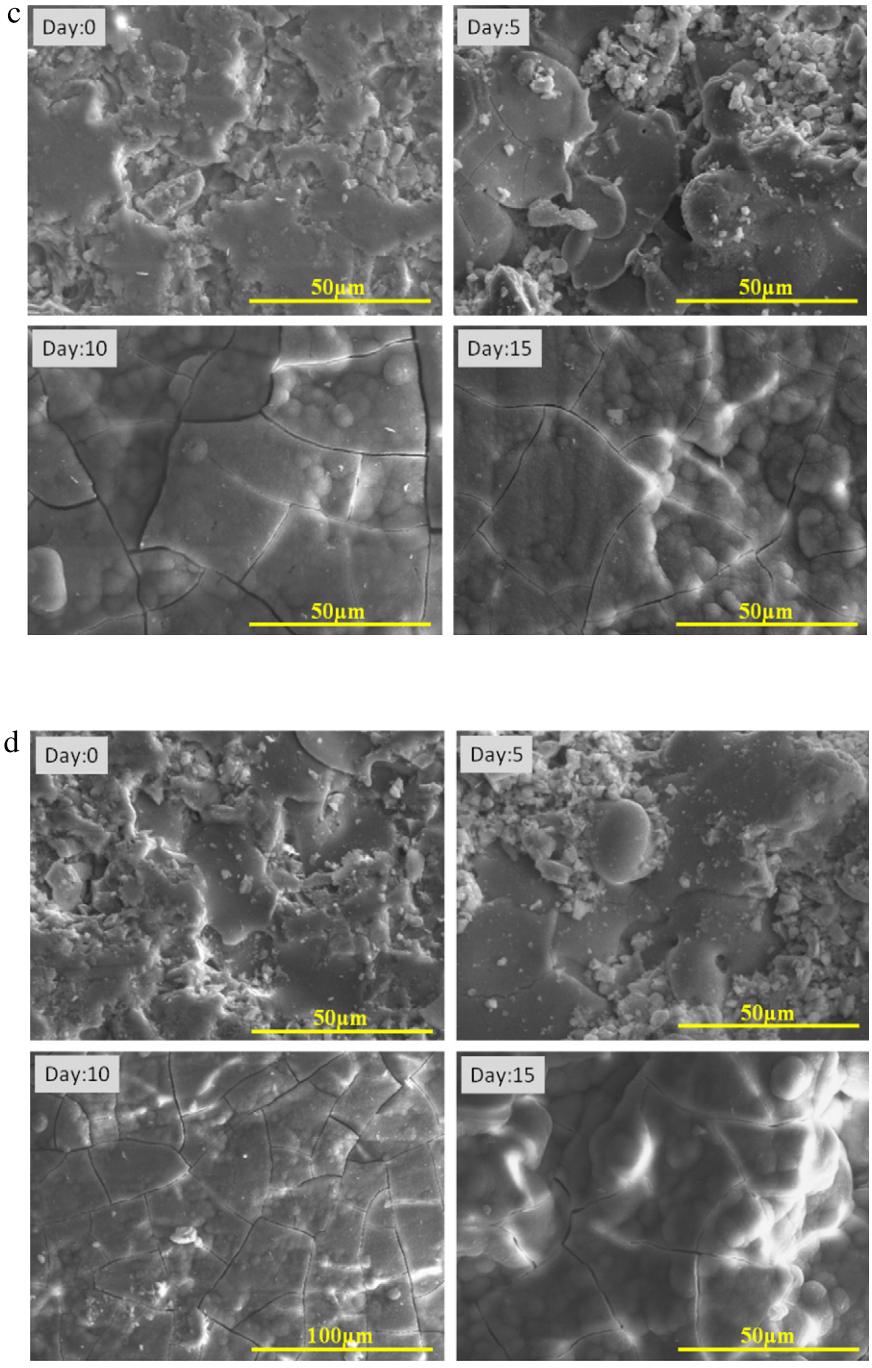

Fig. 10 – (*continued*)

3.4. *Cell culture test*

The cells used in the culture test were the marrow stromal cells (MSCs) of male SD rats. Fig. 12(a) shows fluorescence photographs of the MSCs after being seeded onto the HA and YSZ reinforced HA coating surfaces. The fluorescence microscopic images revealed that the seeded MSCs had spread well and were seen clearly, indicating good livelihood and also that in general all the coating samples were non-toxic for the cultures. The MSCs density as visualized by cell staining showed that these cells grow well after seeding onto the coating surface for 24 h and was found to drastically increase for 48 h of culture of the YSZ reinforced samples compared to the pure HA coatings. Indeed, the SEM investigation (Fig. 12(b)) results revealed that the cells adhered (for both 24 and 48 h) and exhibited a normal elongated and spread-out morphology as those cultured on cell culture surfaces. All the YSZ reinforced coating samples seemed to highly promote the cell adhesion. Overall, the culture revealed that the seeded cells had spread well and the pseudopods were clearly seen, indicating the cytocompatibility of the coating materials.

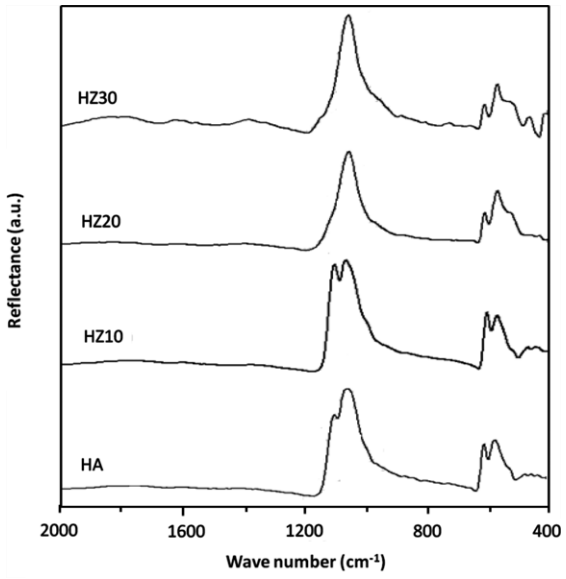

Fig. 11 – Fourier transform infrared spectra of HA, HZ10, HZ20 and HZ30 coatings after immersion in SBF solution at 10 days of immersion.

4. Summary and conclusions

In the present work, gas tunnel type plasma spray torch was successfully employed to produce HA and YSZ reinforced HA coatings i.e. Hydroxyapatite (HA), Hydroxyapatite and 10 wt% YSZ (HZ10), Hydroxyapatite and 20 wt% YSZ (HZ20) and Hydroxyapatite and 30 wt% YSZ (HZ30) on stainless steel substrates. The coating properties such as the phase formation, microstructure and porosity were examined along with its mechanical properties such as microhardness and sliding wear rates. For the aspect of bioactivity, electrochemical corrosion behavior and in vitro apatite layer formation were tested in conventional simulated body fluid (c-SBF) solution. Also the cytocompatibility of the coatings was investigated by using green fluorescent protein (GFP)-labeled marrow stromal cells (MSCs). According to the obtained results of these tests the following conclusions can be drawn:

1. The reinforcement of YSZ in HA significantly reduced the porosity and consequently increased the coating hardness and enhanced the adhesive strength.
2. The sliding wear rate of the coatings was drastically reduced with respect to reinforced YSZ content in HA coatings.
3. The potentiodynamic polarization and impedance measurements showed that YSZ reinforced HA coatings have superior corrosion resistance compared to the pure HA coatings in SBF solution.
4. *In-vitro* SBF immersion results showed the onset of apatite formation on the surface of all the coatings, after 10 days of immersion except for 10% YSZ reinforced HA coating.
5. The reinforced YSZ coatings are non-cytotoxic materials, having improved cell adhesion, attachment and proliferation in cell culture tests after 48 h.

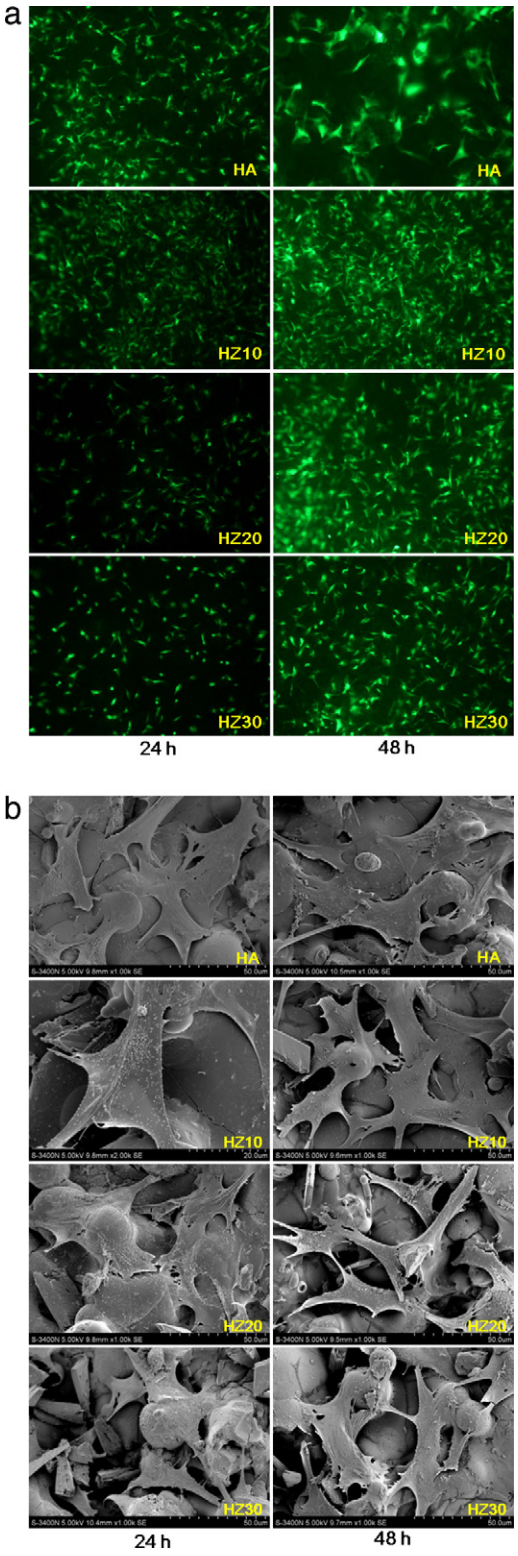

Fig. 12 – (a) Fluorescence and (b) scanning electron microscope images of marrow stromal cell growth on HA and YSZ reinforced HA coating surfaces.

Acknowledgments

The authors (S.Y, A.K and B.S) would like to express their sincere gratitude to Japan Society for the Promotion of Science

(JSPS). Also the authors kindly acknowledge Dr. Guoxian Pei, Dr. Long Bi and Dr. Shu He of Department of orthopedics, Xijing Hospital, The Fourth Military Medical University, PR China for their help rendered in the cell culture analysis.

REFERENCES

Ahn, S.A., Choi, Y.S., Kim, J.G., Han, J.G., 2002. A study on corrosion resistance characteristics of PVD Cr–N coated steels by electrochemical method. Surf. Coat. Technol. 150 (2–3), 319–326.

Arata, Y., Kobayashi, A., 1986. Application of gas tunnel to high energy density plasma beams. J. Appl. Phys. 59 (9), 3038–3044.

Blahoslav, J. Kolman, Karel, Neufuss, Jan, Ilavský, Jiří, Dubský, Pavel, Chráska, 1999. Chemical inhomogeneity of silicates treated by plasma spraying. J. Anal. At. Spectrom. 14, 471–473.

Chang, E., Chang, W.J., Wang, B.C., Yang, C.Y., 1997. Plasma spraying of zirconia-reinforced hydroxyapatite composite coating on titanium. J. Mater. Sci. 8, 193–200.

Chatzistavrou, X., Zorba, T., Chrissafis, K., Kaimakamis, G., Kontonasaki, E., Koidis, P., 2006. Influence of particle size on the crystallization process and the bioactive behavior of a bioactive glass system. J. Therm. Anal. Calorim. 85, 253–259.

Chon, Bang Yen, Chang, Edward, 2002. Plasma-sprayed zirconia bond coat as an intermediate layer for hydroxyapatite coating on titanium alloy substrate. J. Mater. Sci. Mater. Med. 13 (6), 589–595.

Chou, B.Y., Chang, E., 2002. Plasma-sprayed hydroxyapatite coating on titanium alloy with ZrO_2 second phase and ZrO_2 intermediate layer. Surf. Coat. Technol. 153 (1), 84–92.

Chou, B.Y., Chang, E., Yao, S.Y., Chen, J.M., 2002. Phase transformation during plasma spraying of hydroxyapatite–10wt% zirconia composite coating. J. Am. Ceram. Soc. 85 (3), 661–669.

Damyanova, S., Pawelec, B., Arishtirova, K., Martinez Huerta, M.V., Fierro, J.L.G., 2008. Study of the surface and redox properties of ceria-zirconia oxides. Appl. Catal. A 337, 86–96.

Ding, S.J., Ju, C.P., Chern Lin, J.H., 2000. Morphology and immersion behavior of plasma-sprayed hydroxyapatite/bioactive glass coatings. J. Mater. Sci. Mater. Med. 11 (3), 183–190.

Dong, Yang Lin, Yu, Tao Zhao, 2011. Preparation of novel hydroxyapatite/yttria-stabilized-zirconia gradient coatings by magnetron sputtering. Adv. Eng. Mater. 13 (1–2), B18–B24.

Fu, L., Khor, K.A., Lim, J.P., 2002. Effects of yttria stabilized zirconia on plasma sprayed hydroxyapatite/yttria stabilized zirconia composite coatings. J. Am. Ceram. Soc. 85 (4), 800–806.

Geesink, R.G.T., Groot, K., Klein, C., 1987. Chemical implant fixation using hydroxyapatite coatings. Clin. Orthop. 225, 147–170.

Gu, Y.W., Khor, K.A., Pan, D., Cheang, P., 2004. Activity of plasma sprayed yttria stabilized zirconia reinforced hydroxyapatite/Ti–6Al–4V composite coatings in simulated body fluid. Biomaterials 25 (16), 3177–3185.

Gurbhinder, Singh, Surendra, Singh, Satya, Prakash, 2011. Surface characterization of plasma sprayed pure and reinforced hydroxyapatite coating on Ti6Al4V alloy. Surf. Coat. Technol. 205 (20), 4814–4820.

Huang, H.H., Hsu, C.H., Pan, S.J., He, J.L., Chen, C.H., Lee, T.L., 2005. Corrosion and cell adhesion behavior of TiN-coated and ion–nitrided titanium for dental application. Appl. Surf. Sci. 244, 252–256.

Kokubo, T., Kushitani, H., Sakka, S., Kitsugi, T., Yamamuro, T., 1990. Solutions able to reproduce in vivo surface-structure changes in bioactive glass-ceramic A-W3. J. Biomed. Mater. Res. 24 (6), 721–734.

Lee, T.M., Yang, C.Y., Chang, E., Tsai, R.S., 2004. Comparison of plasma-sprayed hydroxyapatite coatings and zirconia-reinforced hydroxyapatite composite coatings: in vivo study. J. Biomed. Mater. Res. Part A 71 (4), 652–660.

Lim, S.C., Brunton, J.H., 1986. The unlubricated wear of sintered iron. Wear 113, 371–382.

Liu, C., Bi, Q., Matthews, A., 2001. EIS comparison on corrosion performance of PVD TiN and CrN coated mild steel in 0.5 NNaCl aqueous solution. Corros. Sci. 43, 1953–1961.

Lorcardi, B., Pazzaglia, U.E., Gabbi, C., Profilo, B., 1993. Thermal behavior of hydroxyapatite intended for medical applications. Biomaterials 14 (6), 437–441.

Mazzocchi, Mauro, Gardini, Davide, Traverso, Pier Luigi, Faga, Maria Giulia, Bellosi, Alida, 2008. On the possibility of silicon nitride as a ceramic for structural orthopaedic implants. Part II: chemical stability and wear resistance in body environment. J. Mater. Sci. Mater. Med. 19, 2889–2901.

Morks, M.F., 2008. Fabrication and characterization of plasma-sprayed HA/SiO_2 coatings for biomedical application. J. Mech. Behav. Biomed. Mater. 1 (1), 105–111.

Morks, M.F., Kobayashi, A., 2008. Development of ZrO_2/SiO_2 bioinert ceramic coatings for biomedical application. J. Mech. Behav. Biomed. Mater. 1 (2), 165–171.

Morks, M.F., Kobayashi, A., 2007. Influence of gun current on the microstructure and crystallinity of plasma sprayed hydroxyapatite coatings. Appl. Surf. Sci. 253, 7136–7142.

Muller, Frank. A., Muller, Lenka, Caillard, Daniel, Conforto, Egle, 2007. Preferred growth orientation of biomimetic apatite crystals. J. Cryst. Growth 304, 464–471.

Nal, U., Sordelet, D.J., 2000. In-plane tensile strength and residual stress in thick Al_2O_3 coatings on aluminum alloy. Scr. Mater. 42 (7), 631–636.

Nancy, Pleshko, Adele, Boskey, Richard, Mendelsohn, 1991. Novel infrared spectroscopic method for the determination of crystallinity of hydroxyapatite mineral. Biophys. J. 60, 786–793.

Nie, X., Leyland, A., Matthews, A., 2000. Deposition of layered bioceramic hydroxyapatite/TiO_2 coatings on titanium alloys using a hybrid technique of micro-arc oxidation and electrophoresis. Surf. Coat. Technol. 125 (1–3), 407–414.

Rabinowicz, E., 1965. Friction and Wear of Materials. Wiley, New York.

Sergo, V., Sbaizero, O., Clarke, D.R., 1997. Mechanical and chemical consequences of the residual stresses in plasma sprayed hydroxyapatite coatings. Biomaterials 18 (6), 477–482.

Sun, L., Berndt, C.C., Gross, K.A., Kucuk, A., 2001. Material fundamentals and clinical performance of plasma-sprayed hydroxyapatite coatings: a review. J. Biomed. Mater. Res. 58 (5), 570–592.

Weng, J., Liu, X., Zhang, X., Ji, X., 1994. Thermal decomposition of hydroxyapatite structure induced by titanium and its dioxide. J. Mater. Sci. Lett. 13, 159–161.

Witek, S.R., Buttler, E.D., 1985. The grain boundary microstructure of a commercial 97% alumina, and the effect of ZrO_2/Y_2O_3 additions. J. Mater. Sci. Lett. 4, 1412–1414.

Xuebin, Zheng, Minhui, Huang, Chuanxian, Ding, 2000. Bond strength of plasma-sprayed hydroxyapatite/Ti, composite coatings. Biomaterials 21, 841–849.

Yoo, Yun Ha, Le, Diem Phuong, Kim, Jung Gu, Kim, Sun Kyu, Vinh, Pham Van, 2008. Corrosion behavior of TiN, TiAlN, TiAlSiN thin films deposited on tool steel in the 3.5 wt% NaCl solution. Thin Solid Films 516 (11), 3544–3548.

Younesi, M., Bahrololoom, M.E., Fooladfar, H., 2010. Development of wear resistant NFSS–HA novel biocomposites and study of their tribological properties for orthopaedic applications. J. Mech. Behav. Biomed. Mater. 3 (2), 178–188.

Zhang, J., Alpas, A.T., 1993. Wear regimes and transitions in Al_2O_3 particulate-reinforced aluminum alloys. Mater. Sci. Eng. A 161, 273–284.